

Study of dynamics in unsteady flows using Koopman mode decomposition

Hassan Arbabi* and Igor Mezić

*University of California, Santa Barbara
Santa Barbara, 93106, CA, USA*

(Dated: April 5, 2017)

The Koopman Mode Decomposition (KMD) is a data-analysis technique which is often used to extract the spatio-temporal patterns of complex flows. In this paper, we use KMD to study bifurcations of the lid-driven flow in a two-dimensional square cavity based on rigorous theorems related to the spectrum of the Koopman operator. We adopt a new computational algorithm, which is capable of detecting true Koopman modes and eigenvalues in post-transient flows with mixed spectra. Properties of the Koopman operator spectrum are linked to the sequence of bifurcations occurring between $Re = 10000$ and $Re = 30000$, and changing the flow nature from steady to aperiodic. The associated Koopman modes show remarkable robustness even as the temporal nature of the flow is changing substantially. We observe that KMD outperforms the Proper Orthogonal Decomposition in reconstruction of the flow, as long as quasi-periodic features are present in the flow.

I. INTRODUCTION

In 1931, Bernard Koopman offered a new formulation of Hamiltonian mechanics based on the theory of Hilbert spaces [1]. In his formulation, the central object was a linear transformation, called the Koopman operator, which described the time evolution of observations on a Hamiltonian system. The potential applications of Koopman's work to general theory of dynamical systems went mostly unrecognized for a long time, until it was brought to attention, and further developed in the context of spectral analysis and dissipative systems [2, 3]. In particular, Ref. 3 presented a linear expansion to describe the temporal evolution of observables on a nonlinear dynamical system in terms of the eigenfunctions and eigenvalues of the Koopman operator. This expansion, known as the Koopman Mode Decomposition (KMD), also introduced the concept of Koopman modes, which are projection of observable evolution onto eigenfunctions of the Koopman operator, and give spatial "shapes" that evolve exponentially in time - with exponents which could be complex numbers. Since then, KMD has been used as a tool of data-driven analysis with applications ranging from power network stability analysis to pattern detection in neural networks [4–9].

In high-dimensional systems like fluid flows, direct analysis of the state space is computationally prohibitive and one often relies on the data-driven methods to extract the underlying spatio-temporal features from data obtained by numerical simulation or experiment. For this purpose, the KMD was introduced to fluid mechanics by Rowley *et al.* [10], with an application to the problem of

jet in cross flow. Rowley *et al.* showed how KMD can extract various oscillation frequencies and their associated spatial structures from the data. They also discovered the connection between the KMD and the numerical algorithm called Dynamic Mode Decomposition (DMD), which had been proposed by [11]. Since then, KMD and its numerical counterpart DMD, have become popular tools for extraction of physically-relevant time scales and their associated spatial structures in complex flows [12–17].

In the present study, we use KMD to identify the temporal regimes of the lid-driven cavity flow. The dynamical-systems origin of KMD has motivated a number of its applications in study of dynamical phenomena such as stability, bifurcation and transition in flows. Some examples are study of bifurcation and transition in flow past a cylinder [18, 19], detection of significant structures in boundary layer transition [20, 21], bifurcation analysis using parametric DMD [22] and identification of flow regimes in thermo-fluid systems using sparse sensing [23]. The distinction of our work from the previous studies is that our methodology is rigorously connected to the theory of Koopman operator for post-transient flows. This connection is two-fold: The KMD algorithm that we use is based on the harmonic averaging for computation of Koopman spectrum which has proven convergence properties [24] and second, we use the connection between the computed Koopman spectra and the state-space dynamics using the theorems presented in [25]. Those theorems describe the relation between the distribution of the Koopman eigenvalues and the geometry of attractor in the state space of the flow. Consequently, we are able to detect the flow bifurcations by monitoring the qualitative changes in the distribution of computed Koopman eigenvalues. This methodology can be regarded as generalization of the traditional spectral

* harbabi@engr.ucsb.edu

techniques for detecting bifurcations and chaos, including the power spectrum analysis [26] and fundamental frequency analysis [27].

We apply the KMD algorithm to the two dimensional lid-driven cavity flow with regularized lid velocity. Lid-driven cavity flows are known to exhibit a wide range of dynamical behavior including periodic and aperiodic flow at high Reynolds numbers [28–33]. We identify three consecutive bifurcations that change the flow dynamics as the Reynolds number (Re) is increased. The steady laminar flow first becomes periodic, then quasi-periodic, and later exhibits mixed spectra (i.e. including quasi-periodicity and chaos). The basic frequencies of quasi-periodic components in the flow increase with Re , while the structure of associated Koopman modes show little variation in range of $Re \approx 10000 - 22000$ which consists of periodic, quasi-periodic and mixed-spectra regime. In the mixed-spectra regime, the chaotic part of the motion grows with the increase of Re until no periodicity can be detected in the motion for Reynolds numbers as high as 30000. The only Koopman mode that is maintained in the fully chaotic regime is the mean flow (i.e. the Koopman mode associated with zero frequency) which also exhibits robustness in its qualitative structure.

The computation of Koopman modes and eigenvalues has seen a lot of algorithmic and technical advances in the recent years. Most of the contributions in this area has been centered around the DMD-type class of algorithms. Some of the contributions include new variations of DMD which expanded its connection with KMD [34], or enabled application to a wider range of problems [35, 36]. Given the increasingly large and complex data sets that are generated by simulations and experiments, DMD has also been extended to handle larger data sets [37, 38], different sampling techniques [38–40] and noise [41].

In the present study, we adopt a new algorithm from Laskar [42] to compute the Koopman modes and eigenvalues. The spectrum of the Koopman operator lies on the imaginary axis for post-transient flows and therefore, a classical technique, known as *harmonic averaging*, can be used to compute the Koopman modes [3]. In our algorithm, harmonic averaging is combined with FFT for efficient detection of Koopman frequencies (i.e. Koopman eigenvalues positioned on the imaginary axis) and Koopman modes. In addition, by considering the sensitivity of frequency peaks to variation of averaging time interval, we are able to distinguish the true Koopman eigenvalues from the spurious peaks of the spectra, and therefore detect genuinely-periodic motion in flows that exhibit a combination of quasi-periodicity and chaos.

A key objective of modal decompositions, such as DMD, is to obtain low-dimensional representation of the data from experiments or numerical simulations. Accordingly, several authors have proposed different variations of DMD algorithm to obtain low-dimensional description

of the spatio-temporal features of the flow in an optimal manner [18, 43, 44]. DMD has also been used in a data assimilation approach to obtain a low-dimensional dynamic model of the cylinder wake flow [45]. Here, we study the efficiency of the Koopman modes in representing the cavity flow dynamics by considering the error in the low-dimensional truncations of KMD. Our results show that low-dimensional truncations of KMD provide a more efficient approximation of the flow than the models obtained by truncations of Proper Orthogonal Decomposition (POD), as long as the flow exhibits some periodic and quasi-periodic time-dependence. This is due to the fact that Koopman modes can be complex-valued and thus more suitable for description of motion on periodic and quasi-periodic attractors.

The outline of this paper is as follows. In §II, we review the basics of the Koopman operator theory and describe how the Koopman spectrum and the geometry of the attractor are related. We also point out the connection between the Koopman mode decomposition of different observables such as stream function, velocity field and vorticity. The referenced theorems are presented in appendix A. In §III, The numerical procedures involved in computing the solution of Navier-Stokes equation, and the KMD algorithm are reviewed. In §IV, we present the evolution of the Koopman spectrum as the flow undergoes the transition from steady to chaotic flow. The Koopman modes and eigenfunctions are discussed in §IV B, and the spectral projections of the data are presented in §IV C. We summarize the results and conclude in §V.

II. KOOPMAN OPERATOR THEORY

The Koopman operator theory is a mathematical formalism that relates the observations on a system to its underlying state-space dynamics. For a viscous incompressible flow, the state space is infinite-dimensional, i.e., it consists of all divergence-free smooth vector-fields defined on the flow domain. Studying the trajectories in the state space of such system via classical tools, like Poincaré maps, is computationally expensive or non-viable, since they involve computation or visualization in an appropriate truncation of an infinite-dimensional space. The Koopman operator viewpoint circumvents this problem by focusing on the time evolution of observables rather than state variables. The magnitude of pressure field at a certain point in the flow domain or the total kinetic energy of the fluid are examples of observable on a flow, suited for the Koopman operator analysis. Observables could be multiple-valued as well, like a vector containing the values of velocity at multiple grid points, or even a field of observables such as the vorticity field. One prominent outcome of the Koopman operator theory is the Koopman mode decomposition [3], which

describes the evolution of such observables as a linear combination of Koopman modes, Koopman eigenfunctions and Koopman frequencies, which are all explained below. We briefly review the basic formalism of the theory but the interested reader is referred to the review article [24] and the references therein for a more detailed exposition.

Consider the state space of a flow including all the smooth divergence-free velocity fields defined on the flow domain. The state of the flow, realized by the velocity field \mathbf{u} , evolves in time according to the Navier-Stokes equation written as

$$\partial_t \mathbf{u}(\mathbf{x}, t) = \mathbf{F}(\mathbf{u}(\mathbf{x}, t)). \quad (1)$$

In the case of bounded 2D flows with no-slip boundary condition, such as lid-driven cavity flow, the solution of this system is known to uniquely exist for future times, and furthermore, the flow trajectory asymptotically converges onto a compact subset of the state space [46]. Under such condition, we let g be a complex-valued function on the state space of the flow, i.e., for every state \mathbf{u} , the observable returns the complex value $g(\mathbf{u})$. We call g an *observable* on the flow. The Koopman operator describes how this observable changes with time. More precisely, the Koopman operator at time $\tau \in [0, \infty)$, denoted by U^τ , maps the function g to a new function g^τ such that

$$g^\tau(\mathbf{u}(\mathbf{x}, t)) := U^\tau g(\mathbf{u}(\mathbf{x}, t)) = g(\mathbf{u}(\mathbf{x}, t + \tau)), \quad (2)$$

The Koopman operator is a linear operator by definition ($U(\alpha_1 g + \alpha_2 h) = \alpha_1 U^\tau g + \alpha_2 U^\tau h$ for scalars $\alpha_{1,2}$) and therefore analyzing its spectrum and eigenfunctions gives a comprehensive understanding of its action on observables. An eigenfunction of the Koopman operator is a function on the state space of the flow, similar to g , which evolves linearly with time. Let us denote by ϕ_j the Koopman eigenfunction associated with the Koopman eigenvalue λ_j . Then

$$\phi^\tau(\mathbf{u}) := U^\tau \phi_j(\mathbf{u}) = e^{\lambda_j \tau} \phi_j(\mathbf{u}) \quad (3)$$

In this work, we consider the post-transient flow dynamics, for which, the Koopman eigenvalues are known to lie on the imaginary axis [3]. Therefore, we will be interested in Koopman frequencies, ω_j , related to Koopman eigenvalues through the following,

$$\lambda_j = i\omega_j, \quad \omega_j \in \mathbb{R}. \quad (4)$$

Let us temporarily assume that all the observables lie in the linear span of the Koopman eigenfunctions. Then any observable like g can be expanded in the Koopman eigenfunctions,

$$g(\mathbf{u}) = \sum_{j=1}^{\infty} g_j \phi_j(\mathbf{u}), \quad (5)$$

where the scalar coefficient g_j is given by the projection of observable g onto the Koopman eigenfunction ϕ_j . Since the Koopman operator is linear, we can use Eq. (3) and find a new expression for evolution of observable g in terms of the Koopman eigenfunctions,

$$g^\tau(\mathbf{u}) = U^\tau g(\mathbf{u}) = \sum_{j=1}^{\infty} g_j \phi_j(\mathbf{u}) e^{i\omega_j \tau}. \quad (6)$$

If we replace the single-valued observable g with a vector-valued observable such as \mathbf{g} , and follow the above procedure, the coefficient g_j turns into the vector of coefficients \mathbf{g}_j , and we obtain a similar expansion in the vector form,

$$\mathbf{g}^\tau(\mathbf{u}) := U^\tau \mathbf{g}(\mathbf{u}) = \sum_{j=1}^{\infty} \mathbf{g}_j \phi_j(\mathbf{u}) e^{i\omega_j \tau}, \quad (7)$$

This expansion of observables in terms of Koopman eigenfunctions is the so-called Koopman Mode Decomposition (KMD). The vector \mathbf{g}_j , called the Koopman mode associated with the Koopman frequency ω_j , describes the components of the observable \mathbf{g} obtained by projection of the observable onto the Koopman eigenfunction ϕ_j . As a result, the evolution of \mathbf{g} in time could be described as a linear combination of Koopman modes with oscillating coefficients. We will further explain the nature of this expansion in §II A and Koopman modes in §IV.

The above expansion can be applied to *fields of observables* as well, in which case, the Koopman modes become fields of coefficients. For example, projecting the *velocity field observable* onto a Koopman eigenfunction returns a field of coefficients which can be thought of as a steady velocity field. Note that the velocity field undergoes nonlinear time evolution described by Navier-Stokes equations, but at the same time, the Koopman mode decomposition of the velocity field as an observable, offers a linear expansion in Koopman modes. This seeming paradox between the nonlinear evolution and linear expansion of KMD is resolved once we recall that the expansion in Eq. (7) is essentially infinite-dimensional and therefore it can describe the nonlinear time evolution as well. In the following sections, we explain how the expansion above is related to the asymptotic dynamics of the trajectories in the state space and also remark on the choice of observable for study of the cavity flow.

A. Flow bifurcations and Koopman mode decomposition

It is interesting to see how the expansion in Eq. (7) changes as the flow undergoes bifurcation. We will be interested in detecting the post-transient flow dynamics which is directly related to the type of attractor on which the flow trajectory is evolving. The bifurcations affect the

Koopman eigenvalues, eigenfunctions and modes in the KMD, but here, we only discuss how the change in the distribution of Koopman eigenvalues can be traced back to the occurrence of bifurcations in the flow.

Let us begin by revisiting one key assumption that led to derivation of KMD, namely, the Koopman eigenfunctions spanning the space of observables. For simple attractors such as fixed points, limit cycles and tori, this assumption is valid and therefore the expansion in Eq. (7) can be used to explain the behavior of generic observables. For systems with more complicated attractors, the Koopman eigenfunctions might not exist but there is a more general form of spectral expansion for the Koopman operator, which we will consider shortly.

In case that the trajectory in the state space of the flow evolves on a limit cycle, the post-transient flow shows periodic time dependence. Let us denote the fundamental frequency of the state variable moving on the limit cycle by ω_0 . According to the theorem 1 in Appendix A, the Koopman spectral expansion is given by

$$U^\tau \mathbf{g} = \sum_{k=-\infty}^{\infty} \mathbf{g}_k \phi_k e^{ik\omega_0\tau}. \quad (8)$$

We have dropped the dependence of \mathbf{g} and ϕ_k on the state \mathbf{u} to simplify the notation. In the above, \mathbf{g} and ϕ_k 's are functions defined on the state space of the flow, and the equality holds everywhere on the limit cycle. We can evaluate the above equation for a single initial state: let \mathbf{u}_0 be the state of the flow at time $t = 0$, then the above expansion becomes

$$U^\tau \mathbf{g}(\mathbf{u}_0) = \mathbf{g}(\mathbf{u}(t)) = \sum_{k=-\infty}^{\infty} \mathbf{g}_k \phi_k(\mathbf{u}_0) e^{ik\omega_0\tau}. \quad (9)$$

The term $U^\tau \mathbf{g}(\mathbf{u}_0) = \mathbf{g}(\mathbf{u}(t))$ is the signal (i.e. function of time) generated by observing \mathbf{g} over the trajectory starting at \mathbf{u}_0 . This signal is $2\pi/\omega_0$ -periodic in τ , and not surprisingly, the expansion in (9) is the Fourier-series representation of this periodic signal with Fourier coefficients $\mathbf{g}_k \phi_k(\mathbf{u}_0)$. However, note that \mathbf{g}_k and $\phi_k(\mathbf{u}_0)$ are not just Fourier coefficients but also properties of the dynamical system which are independent of the simulation or experimental setup. We will expand more on the role of eigenfunctions and modes in §IV.

The point-evaluated expansion in Eq. (9) is more suitable for the study of fluid flows than the function expansion in Eq. (8). This is due to the fact that each flow simulation or experiment, provides us with only a single trajectory in the state space and direct evaluation of the Koopman eigenfunctions on arbitrary regions of state space is not practical. In case of post-transient flows, however, the ergodicity condition allows us to construct and visualize the Koopman eigenfunctions on the attractor using the signals coming from as few as one trajectory. We will use this fact to construct and visu-

alize the eigenfunctions on periodic and quasi-periodic attractors in §IV.

In the case of quasi-periodic flow, the trajectory in the state space converges onto m -dimensional torus and the time series generated by measuring an observable exhibits quasi-periodic time-dependence with multiple frequencies. Let $\boldsymbol{\Omega} = [\omega_1, \omega_2, \dots, \omega_m]^T$ denote the vector of frequencies for the quasi-periodic motion on the torus. The Koopman mode decomposition (theorem 2 in Appendix A) becomes

$$U^\tau \mathbf{g} = \sum_{\mathbf{k} \in \mathbb{Z}^m} \mathbf{g}_{\mathbf{k}} \phi_{\mathbf{k}} e^{i\mathbf{k} \cdot \boldsymbol{\Omega} \tau}. \quad (10)$$

Again, we can evaluate this expansion for some reference state \mathbf{u}_0 on the attractor at time $t = 0$ and obtain a generalized Fourier-series expansion for the quasi-periodic time series of observations on \mathbf{g} ,

$$U^\tau \mathbf{g}(\mathbf{u}_0) = \sum_{\mathbf{k} \in \mathbb{Z}^m} \mathbf{g}_{\mathbf{k}} \phi_{\mathbf{k}}(\mathbf{u}_0) e^{i\mathbf{k} \cdot \boldsymbol{\Omega} \tau}. \quad (11)$$

This means that the time series of the flow can be expressed as sum of the periodic signals with frequencies that are integral combination of the basic frequencies in $\boldsymbol{\Omega}$. The converse of the above statement is also true, in the sense that if the Koopman spectrum of observables has only a number of basic frequencies and their combinations, then the flow trajectory must be evolving on a torus-shaped attractor in the state space. More precisely, the *representation theorem* from the ergodic theory states that if the post-transient flow dynamics is ergodic and smooth, the Koopman operator having only discrete spectrum implies that the motion in the state space is conjugate to rotation on a torus [47]. This classic result combined with numerical KMD algorithm of the next section gives a practical framework for detecting motion on tori in high-dimensional systems.

For post-transient flows with chaotic behavior, the evolution of observables cannot be described solely based on the Koopman eigenfunctions. In such systems, the action of Koopman operator on the space of observables is not analogous to finite-dimensional operators, and Koopman eigenfunctions might not even exist. Despite this, the spectral theory of normal operators [48] provides us with a general form of spectral expansion for the Koopman operator. For post-transient flows, this expansion can be written as [3]

$$U^\tau \mathbf{g} = \sum_{k=1}^{\infty} \mathbf{g}_k \phi_k e^{i\omega_k \tau} + \int_{-\infty}^{\infty} e^{i\alpha\tau} \tilde{\mathbf{g}}(\alpha) \rho(\alpha) d\alpha. \quad (12)$$

The first term on the right-hand-side is the contribution of discrete spectrum which corresponds to the quasi-periodic component of the motion. For fully chaotic systems (e.g. chaotic Lorenz attractor) this term vanishes except for $\omega_k = 0$ which is associated with the ergodic

(infinite-time) average of the observable. The second term on the right-hand-side is the contribution of the so-called continuous spectrum of the Koopman operator. Roughly speaking, $i\alpha$ with $\alpha \in (-\infty, \infty)$, denotes a continuum of eigenvalues distributed along the imaginary axis. The spectral density $\rho(\alpha)$ indicates how strong the contribution of frequency α is in the evolution of the observable. Similar to the Koopman mode \mathbf{g}_j , $\tilde{\mathbf{g}}(\alpha)$ is the component of function \mathbf{g} that oscillates with frequency α .

B. Choice of observables and the relationship between their Koopman modes

The next question that we consider is the choice of observables to be used in dynamical analysis of cavity flow. This question is important since applying KMD to an observable reveals only the Koopman eigenvalues that are present in the expansion of that observable. Furthermore, one can use the relationship between the Koopman modes of different observables to reduce the computational cost of the analysis. The propositions in Appendix A help us understand the relationship between the KMD of different observables like velocity and stream function. They assert that if two observables are related through a linear operator, then their modes are also related via the same linear operator. Consider the field of stream function ψ and the velocity field \mathbf{u} in an incompressible 2D flow. These two observables are related thorough the linear operator $\nabla^\perp := [\partial/\partial y, -\partial/\partial x]^T$, that is, $\mathbf{u} = \nabla^\perp \psi$. Let ψ_j and \mathbf{u}_j denote the Koopman modes of these two observable fields associated with Koopman eigenvalue λ_j , then

$$\mathbf{u}_j = \nabla^\perp \psi_j, \quad j = 1, 2, 3, \dots \quad (13)$$

A similar relationship could be established between the Koopman modes of the vorticity field, denoted by ω_j , and those of the velocity field,

$$\omega_j = \nabla \times \mathbf{u}_j, \quad j = 1, 2, 3, \dots \quad (14)$$

This further implies that applying KMD to either of the these observable fields yields the same Koopman eigenvalues as long as none of the modes lie in the null space of the linear operator.

The knowledge of any of the above observable fields, i.e., stream function, velocity field or vorticity, uniquely determines the state of the system and therefore it can be used to elicit the Koopman spectrum of all other observables of interest. Thus we conclude that applying KMD to any of these fields would give us the information which is sufficient to detect the flow bifurcations. In the dynamical analysis of the cavity flow, we choose the stream function as the primary observable for the application of KMD since its Koopman modes and eigenvalues

are least expensive to compute. The Koopman modes of velocity and vorticity are then computed using Eq. (13) and (14).

III. NUMERICAL METHODS

A. Numerical simulation of incompressible flow inside a square cavity

The computational model of the lid-driven cavity flow consists of an incompressible viscous flow inside the square domain $[-1, 1]^2$. The domain boundaries are stationary walls, except the top lid (at $y = 1$) which moves with a regularized velocity profile,

$$u_{lid} = (1 - x^2)^2, \quad x \in [-1, 1]. \quad (15)$$

This boundary condition ensures that the velocity field is continuous and divergence-free in the top corners ($x = \pm 1, y = 1$). The incompressibility of the flow allows us to use the stream function formulation of the Navier-Stokes equation,

$$\frac{\partial}{\partial t} \nabla^2 \psi + \frac{\partial \psi}{\partial y} \frac{\partial}{\partial x} \nabla^2 \psi - \frac{\partial \psi}{\partial x} \frac{\partial}{\partial y} \nabla^2 \psi = \frac{1}{Re} \nabla^4 \psi, \quad (16)$$

subject to two types of boundary condition on the stream function,

$$\psi \Big|_{\partial\Omega} = 0 \quad \text{and} \quad \frac{\partial \psi}{\partial n} \Big|_{\partial\Omega} = u_w, \quad (17)$$

where the wall velocity u_w is zero everywhere except at the top wall, where $u_w(y = 1) = u_{lid}$.

For spatial discretization, we have used the Chebyshev-spectral collocation method described in Ref. 49. The solution to the above PDE is approximated by a polynomial of order N in each spatial direction. This polynomial is characterized by its values at the Chebyshev points,

$$(x_i, y_j) = \left(\cos\left(\frac{i\pi}{N}\right), \cos\left(\frac{j\pi}{M}\right) \right) \quad (18)$$

$$i = 0, 1, \dots, N, \quad j = 0, 1, \dots, M.$$

Given the polynomial approximation and the prescribed boundary condition in (17), we use the transformed variable $q(x, y)$ defined by

$$\psi(x, y) = (1 - x^2)(1 - y^2)q(x, y). \quad (19)$$

which satisfies the Dirichlet boundary condition identically, and turns the Neumann boundary condition into Dirichlet boundary condition, i.e.,

$$q(\pm 1, y) = q(x, -1) = 0, \quad (20)$$

$$q(x, +1) = -\frac{1}{2}u_{top}(x). \quad (21)$$

For the temporal discretization of the ordinary differential equations on $q(x_i, y_i)$, we have used the second-order Crank-Nicholson scheme for the diffusion terms and second-order Adams-Bashforth discretization for the convection terms. The flow solutions studied in this work are computed using zero initial velocity in the cavity domain. The numerical solutions of the steady flow obtained by our method agree with the results reported in Ref. 28. There is also agreement on the time periods of the periodic flows between the two studies. To the best of our knowledge, however, there are no reported benchmark solutions for quasi-periodic or aperiodic flow.

B. Koopman mode decomposition via harmonic averaging and DFT

Let us start by assuming that the Koopman frequencies in the decomposition of the observable \mathbf{g} are known beforehand and denote them by ω_j , $j = 1, 2, 3, \dots$. Then we can directly compute the Koopman modes of this observable using the harmonic average [24],

$$\mathbf{g}_j = \lim_{T \rightarrow \infty} \frac{1}{T} \int_0^T \mathbf{g}(\tau) e^{-i\omega_j \tau} d\tau. \quad (22)$$

The above limit is known to exist for almost every initial condition under the common assumption that the dynamics on the attractor is preserving a measure [50]. The time series obtained by experiments and simulations usually consist of sampled values at discrete times over finite-length intervals. Therefore approximating the Koopman modes of the numerical data using this formula requires two steps. First, this integral should be estimated by an integral over a finite interval,

$$\mathbf{g}_j^T = \frac{1}{T} \int_0^T \mathbf{g}(\tau) e^{-i\omega_j \tau} d\tau. \quad (23)$$

In the second step, the finite-time integral should be approximated by a sum over the discrete-time samples of the data, such as

$$\mathbf{g}_j^N = \frac{1}{N} \sum_{k=0}^N \mathbf{g}(k) e^{-i\omega_j \tau_k}, \quad (24)$$

where $\mathbf{g}(k)$ is the value of observable at the sampling time τ_k , and w_k is the appropriate weight for integration. The error associated with the first step depends on the dynamical behavior of systems; for quasi-periodic flows the error decreases as T^{-1} [51], and for typical chaotic attractors it decays as $T^{-1/2}$ [52]. The error associated with the second step, depends on the sampling and could be often reduced by increasing the sampling rate or using higher-order approximations.

It still remains to compute the Koopman frequencies. A simple solution is to approximate ω_j 's with the Fourier

frequencies. Let N be the (even) number of observations on \mathbf{g} that we have made over the time interval T , and let $\Delta\tau$ denote the sampling time, i.e., $\Delta\tau = T/(N-1)$. The Fourier frequencies are given by

$$\Omega_j = \frac{2\pi j}{N\Delta\tau}, \quad j = -\frac{N}{2}, -\frac{N}{2}+1, \dots, 0, \dots, \frac{N}{2}-1, \quad (25)$$

Accordingly, computation of the Koopman modes in (24) reduces to the computing the temporal Discrete Fourier Transform (DFT) of the observations, defined as

$$\hat{\mathbf{g}}_j = \frac{1}{N} \sum_{k=0}^{N-1} \mathbf{g}(k) e^{-i\Omega_j k \Delta\tau}. \quad (26)$$

The Fourier amplitude $\hat{\mathbf{g}}_j$ is non-zero, in principle, for all Ω_j 's, however, when N is large enough, we expect $\hat{\mathbf{g}}_j$ to be close to zero for Ω_j that are not Koopman frequencies, and approximate the Koopman modes for Ω_j 's close to the Koopman frequencies. As such, the Fourier amplitudes offer an approximation to the Koopman modes, given that the DFT is performed over a sufficiently long sequence of observation. Note that DFT is also shown to be equivalent to DMD when applied to a linearly-independent sequence of data snapshots with zero mean [18]. The advantage of using DFT to find the Koopman modes lies in its relative simplicity and the availability of fast algorithms for its implementation, i.e., Fast Fourier Transform (FFT) algorithms. In general, however, the Koopman frequencies do not coincide with the Fourier frequencies since the Koopman frequencies depend on the dynamics whereas Fourier frequencies are prescribed by the sampling rate and observation interval.

In this work, we adopt the adaptive frequency-extraction algorithm which was introduced (in a different context) by Laskar [42]. We first use FFT to estimate the value of a Koopman frequency associated with the most dominant Koopman mode. Then we use the direct harmonic averaging, possibly with data windowing, to improve this estimate and compute the associated Koopman mode. We then extract the contribution of this mode from the data, and then repeat the same steps to compute the Koopman frequency associated with the next dominant mode.

C. Algorithm for computing the Koopman frequencies and modes

Let $\{\mathbf{g}^{\tau_0}, \mathbf{g}^{\tau_1}, \dots, \mathbf{g}^{\tau_n}\}$ be the set of observations on the vector-valued observable \mathbf{g} , made on uniformly-spaced time instants $\{\tau_0 = 0, \tau_1, \dots, \tau_{n-1}, \tau_n = T\}$. The data matrix \mathbf{G} is defined as

$$\mathbf{G} = [\mathbf{g}^{\tau_0} | \mathbf{g}^{\tau_1} | \mathbf{g}^{\tau_2} | \dots | \mathbf{g}^{\tau_n}]. \quad (27)$$

Also let $\|\cdot\|$ denote an appropriate vector norm on the observable \mathbf{g} . The Koopman eigenvalues and modes of \mathbf{g} are computed thorough the following steps:

1. Find a candidate Koopman frequency using FFT.

Apply the row-wise FFT to the data matrix G and find the complex amplitude vectors $\hat{\mathbf{g}}_j$. Find the highest distinguished peak in the plot of $\|\mathbf{g}_j\|$ versus Ω_j . Denote the Fourier frequency associated with this peak, by Ω^* . This is the first approximation of a Koopman frequency. If there are no distinguished peaks proceed to step 6.

2. Compute the Koopman frequency using filtered harmonic averaging.

Search in the vicinity of Ω^* for the frequency ω_k that maximizes the $\|\cdot\|$ -norm of the filtered harmonic average

$$\mathbf{g}^* = \int_0^T \mathbf{g}(\tau) e^{-i\omega_k \tau} \chi(\tau) d\tau, \quad (28)$$

where $\chi(\tau)$ is the Hann windowing function,

$$\chi(\tau) = \frac{1}{T} \left(1 - \cos \frac{2\pi\tau}{T}\right). \quad (29)$$

The frequency ω_k is an approximation of a Koopman frequency.

3. Compute the associated Koopman mode using harmonic averaging.

Compute the Koopman mode associated with ω_k by re-evaluating (28) with the constant weight function $\chi(\tau) = 1/T$. Denote the Koopman mode by \mathbf{g}_k .

4. Subtract the contribution of the Koopman frequency from the data.

The contribution of ω_k to the data is given by the matrix

$$\mathbf{G}_k = [\mathbf{g}_k | \mathbf{g}_k e^{i\omega_k T/n} | \mathbf{g}_k e^{i\omega_k 2T/n} | \dots | \mathbf{g}_k e^{i\omega_k T}]. \quad (30)$$

Subtract \mathbf{G}_k from the data matrix \mathbf{G} .

5. Repeat the steps 1-4 using the data obtained in step 4.

6. Present the evolution of observable as sum of contributions from ω_k 's.

The Koopman mode decomposition of observable \mathbf{g} computed by the above process is

$$\mathbf{g}^\tau := U^\tau \mathbf{g} = \sum_{k=1}^m \mathbf{g}_k e^{i\omega_k \tau} + \sum_{j=0}^{n-1} \tilde{\mathbf{g}}_j e^{i\Omega_j \tau}, \quad (31)$$

where m is the number of Koopman frequencies found thorough step 1 to 4 and $\tilde{\mathbf{g}}_k$'s denote the complex amplitudes computed by applying FFT to the data obtained in step 4.

The above expansion is the numerical approximation of the Koopman mode expansion, such as (9) and (11), with the exception that we have absorbed the scalar values of $\phi_k(\mathbf{u}_0)$'s into the Koopman modes. Consider the application of the algorithm to the time series generated by measuring a vector-valued observable in a flow experiment or simulation. If the state space dynamics is periodic or quasi-periodic, the harmonic average in step 3 converges to the Koopman modes as $T \rightarrow \infty$ if ω_k is a Koopman frequency, and it decays to zero if the ω_k is not a Koopman frequency. Moreover, the rate of convergence is proportional to $1/T$ [51] and it can be further enhanced using the averaging weight suggested by [53]. The windowing filter in (29) also facilitates detecting frequency peaks that are positioned close to each other [27]. Therefore, we expect that for sufficiently large T , the expansion in Eq. (31) would be a good approximation of the Koopman mode expansion in Eq. (9) or (11).

In the fully chaotic flows, the Koopman operator has no eigenvalues other than zero and the only Koopman mode would be the infinite-time average of the observable (i.e., harmonic average at zero frequency). As a result, the harmonic averaging in step 3 converges to zero for all non-zero frequencies as $T \rightarrow \infty$. A precarious situation arises when the Koopman operator has mixed spectra, that is, both eigenvalues and continuous spectrum. The evolution of a typical observable in such flows consists of both periodic and chaotic components, and admits the general form of KMD in Eq. (12). Application of the harmonic averaging to flows with mixed spectra needs some extra processing because if it is applied at a frequency which is not in the Koopman spectrum, it vanishes as $T \rightarrow \infty$, but the decaying might be slow and undetectable, which results in computation of spurious Koopman modes.

Here, we make the assumption that the chaotic component of the flow is strongly mixing, which implies that the harmonic average decays as $1/\sqrt{T}$ as $T \rightarrow \infty$ [52]. Using this assumption, we are able to set a threshold to distinguish between the genuine Koopman modes and the spurious ones as follows: In computing the harmonic average in the step 3, the integration time T is varied to check the robustness of the peak. Using the strong mixing assumption, we discard the peaks that show 50% or more decay when the integration interval is quadrupled. The remaining peaks are deemed robust and correspond to Koopman frequencies that make the first term on the right-hand-side of (31), and the remainder is the DFT expansion of the chaotic component of the observable. Note that computing the decay rate of time averages to detect chaos has been previously suggested by several authors [54, 55].

We have applied the above algorithm to the vector of the stream function values at the computational grid points given in Eq. (19). The Koopman modes of velocity and vorticity are subsequently computed from the modes

of stream function via Eqs. (13) and (14). The spectrum of lid-driven cavity varies from discrete spectrum (periodic and quasi-periodic) to mixed and continuous spectra in high Reynolds numbers. To detect the robust peaks in the case of mixed spectrum, we have varied the time interval of observation between 1000 and 4000 characteristic time units. The characteristic time unit, denoted by t_c , is defined as

$$t_c = \frac{L_R}{U_R} \quad (32)$$

where L_R and U_R are chosen to be, respectively, the half of the cavity side length and maximum velocity on the top lid. We have used the kinetic-energy norm of the Koopman modes as the vector norm in the above algorithm. We regard a frequency as having a *distinguished* peak (in step 1 of the algorithm), if it contains at least twice the kinetic energy of each of its neighbors.

IV. CAVITY FLOW DYNAMICS AND KMD

A. Koopman spectrum

We use the theory in §II A to identify the type of the attractor from the computed spectra of the Koopman operator. Figure 1 shows the Koopman spectrum of post-transient flow at four different Reynolds numbers. The representation of the Koopman spectrum in the figure is based on the distribution of the kinetic energy in the observed Koopman frequencies. The horizontal axes show the Koopman frequencies in the non-dimensional form of the Strouhal number,

$$St_j = \frac{\omega_j t_c}{2\pi} \quad (33)$$

where t_c is the characteristic time unit defined in (32). The vertical axes denote the the kinetic-energy norm of the associated velocity modes,

$$\|\mathbf{u}_j\| = \left(\frac{\int_{\Omega} |\mathbf{u}_j|^2 ds}{U_R^2} \right)^{1/2}. \quad (34)$$

The blue circles highlight the frequency peaks that are robust to the variations in the time interval of harmonic averaging and therefore, mark the true Koopman frequencies. The values of those frequencies and their rational dependence are tabulated in Appendix B.

When the Reynolds number is smaller than 10000, the cavity flow induced by regularized lid velocity converges to a steady laminar solution which corresponds to a fixed point in the state space of the flow. The Koopman mode expansion for steady flows is trivial and consists of zero frequency with an associated mode which is the steady flow. At a Reynolds number slightly above 10000, the

steady solution becomes unstable and the numerical solution converges to a time-periodic flow which maintains stability up to $Re = 15000$. The Koopman spectrum in this range consists of extremely sharp and robust peaks at zero and other frequencies that are multiples of a basic frequency.

The basic frequency of periodic flow decreases with the Reynolds number, until at a Reynolds number slightly above 15000, another bifurcation occurs and the solution converges to a quasi-periodic flow. This is easily recognized from the change in the Koopman spectrum; the robust frequency peaks in the range of $Re = 16000 - 18000$ closely resemble the lattice of frequencies described by the KMD of quasi-periodic evolution in (10). For instance, the vector of the basic frequencies for the case of $Re = 16000$, (top right panel in FIG. 1), is $St = [0.1554, 0.2523]$, and every peak marked by a blue circle is a linear combination of these two frequencies with integer coefficients (table I in Appendix B).

The basic frequencies of the quasi-periodic flow also decrease with the Re , but around $Re = 18000$ another bifurcation occurs and the level of energy lying in between the discrete peaks starts to rise dramatically with Re . This amplification of energy content in the background Fourier frequencies is independent of the time interval of KMD computation and therefore we attribute it to the appearance of the continuous spectrum which is associated with chaotic motion in the state space. At the same time, the spectrum still contains a lattice of frequencies that can be traced back to the purely quasi-periodic motion at lower Reynolds numbers (see table I). This observation leads us to conclude that the attractor in the state space of the flow is a cross-product of a tori, responsible for quasi-periodic motion, and a chaotic set which generates the chaotic components. This type of attractor is called skew-periodic in the literature of dynamical systems theory [56]. The energy contained within the continuous spectrum grows with Re and it subsumes the discrete spectrum around $Re=22000$, above which, no robust peaks other than zero frequency are detected. The apparent peaks in the spectrum of such flows ($Re = 30000$ in FIG. 1) decay considerably with the time interval of harmonic averaging and they are dismissed by the criteria introduced in §III C. In this case the state space dynamics is fully chaotic.

The evolution of the Koopman spectrum in FIG. 1 offers a picture of transition to chaos that is consistent with the theory of Ruelle and Takens [57]. According to this theory, the chaotic state of the flow can be reached after one or two Hopf bifurcations from an initially-stable fixed point. Practical evidence for this theory appeared in the experiments on rotating Couette flow and natural convection by Swinney and Gollub [26]. In particular, they detected the flow bifurcations using the power spectrum of velocity measurements at a single point in the flow domain. The transition to chaos was marked by

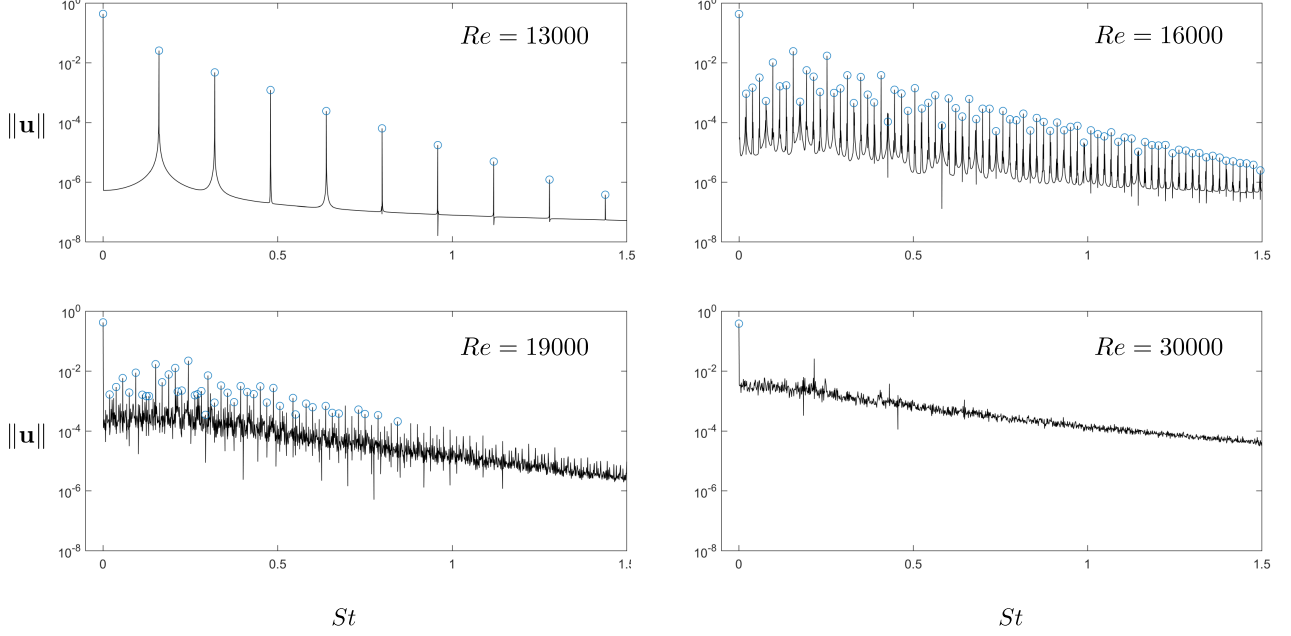


FIG. 1. Koopman spectra of the cavity flow. The blue circles mark the peaks that persist by varying the averaging time and therefore correspond to the discrete Koopman spectrum. For periodic and quasi-periodic flows (the top row) the kinetic energy is distributed in a lattice of discrete spectrum. For flow with mixed spectra (the bottom left), there are robust peaks within a high-energy background of Fourier frequencies, whereas the chaotic flow (the bottom right) has only one Koopman frequency i.e. zero.

the sudden growth of “background noise” in the power spectrum of the quasi-periodic flow. The Ruelle-Takens scenario for transition to chaos seems to be valid for the numerical model of the lid-driven cavity flow. The above results show that the Koopman spectrum can be used as a generalized spectral tool for detection of flow dynamics.

B. Koopman eigenfunctions and the Koopman modes

In this section, we discuss the relationship between the state space dynamics and the evolution of the cavity flow in the physical domain. To this end, we will construct the Koopman eigenfunctions that correspond to periodic and quasi-periodic flow based on the theory presented in [25]. Consider the periodic flow discussed above. We parameterize the limit cycle that corresponds to this flow using the coordinate $s \in [0, 2\pi)$ with $\dot{s} = \omega_1$, where ω_1 is the basic frequency of the limit cycle and its non-dimensional value is $St_1 = 0.1598$ for $Re = 13000$. Recall that the Koopman frequencies are given by $k\omega_1$ with $k \in \mathbb{Z}$. The Koopman eigenfunction associated with the Koopman frequency $k\omega_1$ is

$$\phi_k = e^{iks}, \quad k \in \mathbb{Z}. \quad (35)$$

The eigenfunctions of the quasi-periodic flow are constructed in a similar way. Let $\Theta \in [0, 2\pi]^2$ be the parametrization of the quasi-periodic attractor (i.e. torus) such that the trajectory coordinate evolves according to the linear equation

$$\dot{\Theta} = \Omega, \quad (36)$$

where Ω is the vector of basic frequencies computed by KMD algorithm. The eigenfunction associated with the Koopman frequency $\mathbf{k} \cdot \Omega$ is

$$\phi_{\mathbf{k}} = e^{i\mathbf{k} \cdot \Theta}, \quad \mathbf{k} \in \mathbb{Z}^2 \quad (37)$$

The top row in FIG. 2 and 3 show the Koopman eigenfunctions of the periodic and quasi-periodic flow on an embedded attractor (see Appendix C for details on visualization). The eigenfunction associated with the zero Koopman frequency ($k = 0$ or $\mathbf{k} = 0$) is the invariant of the motion in the state space, i.e., it is constant along the trajectory. On the other hand, the vorticity field observable is a function that assigns a vorticity field on cavity domain to each point on the attractor. The projection of that observable onto the invariant Koopman eigenfunction is a field of coefficients which is the Koopman mode of vorticity associated with zero Koopman

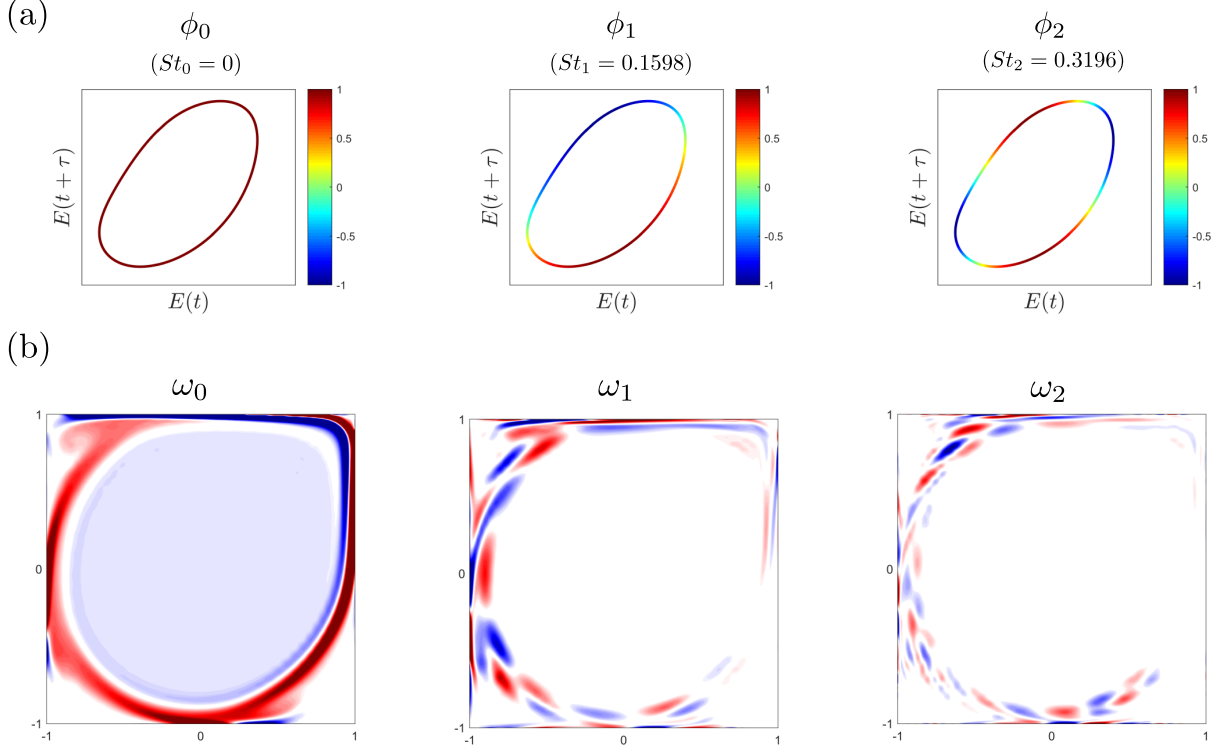


FIG. 2. (a) The (real part of) Koopman eigenfunctions shown as color field on the embedded attractor (limit cycle) of the periodic flow at $Re=13000$, and (b) real part of the associated Koopman modes of vorticity (clockwise rotation shown in red and counterclockwise in blue). The attractor is reconstructed using a 2D delay embedding of kinetic energy (E) with the time delay $\tau = t_c$.

frequency. This mode is also an invariant of the flow in the sense that it does not depend on the initial condition as long as different initial condition lead to the same asymptotic behavior (i.e. converge to the same attractor).

The oscillatory Koopman eigenfunctions ($k \neq 0$ or $\mathbf{k} \neq 0$) introduce a dynamically-induced set of coordinates on the attractor. For the limit cycle, they are periodic functions along the limit cycle. For the torus, however, they reveal the principle directions of motion, which cannot be easily inferred from the data. The temporal evolution of the modes can be interpreted as the change in the value of the eigenfunctions, i.e., as the trajectory moves forward in time its coordinates along the Koopman eigenfunctions evolves linearly with time. This evolution is given by the term $\phi_{\mathbf{k}}(\mathbf{u}(t)) = \phi_{\mathbf{k}}(\mathbf{u}_0)e^{i\omega_{\mathbf{k}}t}$ which is the oscillating amplitude of the mode \mathbf{u}_k in the Koopman mode expansion (11). The evolution of the observable in the physical domain, however, is a superposition of oscillations between the real part and imaginary part of the modes that occurs at the various Koopman frequencies.

The Koopman modes of vorticity associated with largest contribution to the kinetic energy of the flow (i.e.

associated with highest peaks in the spectra) are shown in FIG. 4. The mean flow, which is the Koopman mode associated with zero frequency ($k = \mathbf{k} = 0$), contains the largest share of kinetic energy in all unsteady regimes (panel 1,4,7,10 in figure, counting from the top left to right). It is essentially composed of a rotating central core with smaller corner eddies in the downstream of the moving lead. For fully chaotic flows, the mean flow is the only detected Koopman mode, and its structure is similar to the mean flow of periodic and quasi-periodic flow except for the intensification of the downstream eddy in the bottom right corner.

The oscillatory Koopman modes generally describe oscillations of the flow field variables around the shear layer. Our results show that higher Koopman frequencies are typically associated with modes that have higher wave numbers of spatial variation (e.g. compare panel 2 with 3). An interesting observation is that the oscillatory modes show a remarkable structural robustness; although the Koopman frequencies generally increase with Re , their associated Koopman modes undergo little change. Two examples of such continuation are shown in the figure: panel 2,5 and 8 which correspond to the frequency

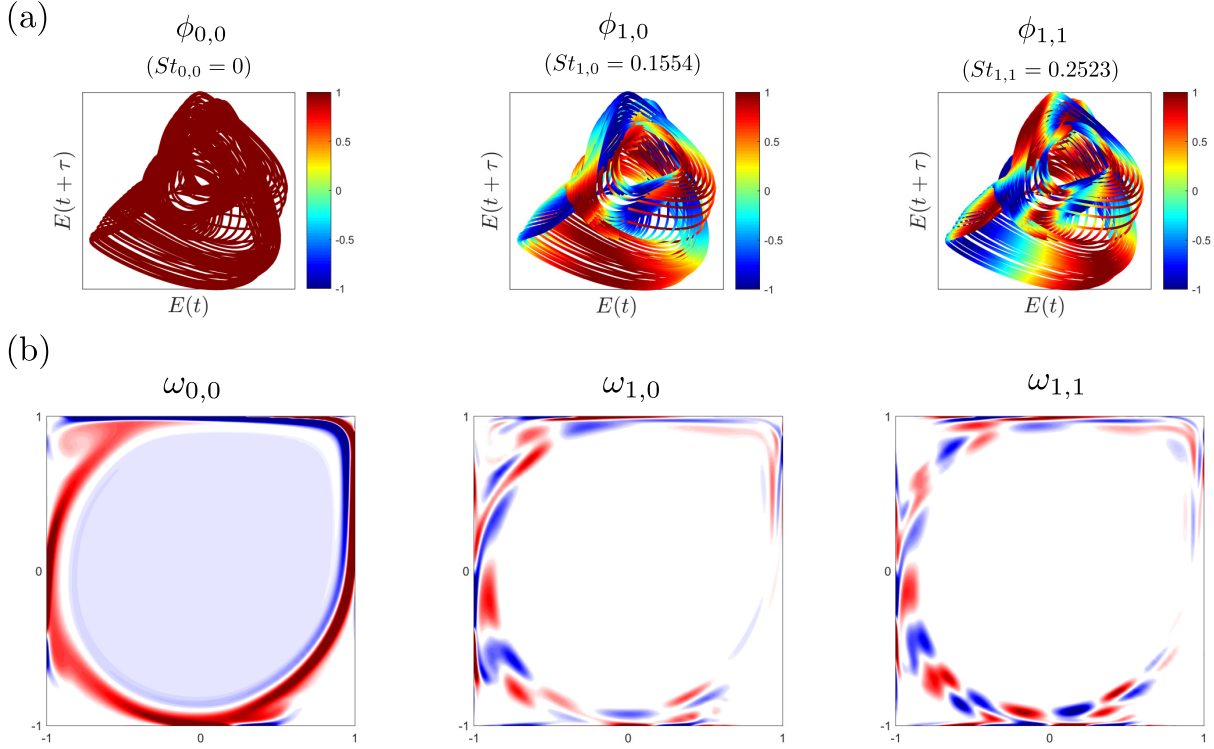


FIG. 3. (a) The (real part of the) Koopman eigenfunctions shown as color field on the embedded attractor (torus) of the quasi-periodic flow at $Re=16000$, and (b) the real part of associated Koopman modes of vorticity (clockwise rotation shown in red and counterclockwise in blue). The attractor is reconstructed using a 3D delay embedding of kinetic energy (E) with the time delay $\tau = 2.4t_c$ (The z -axis is not shown).

ω_1 in periodic, quasi-periodic and mixed-spectra regimes, and panel 6 and 9 associated with the frequency $\omega_1 + \omega_2$ in quasi-periodic and mixed-spectra regimes.

C. Spectral Projections and Proper Orthogonal Decomposition (POD)

We study the efficiency of Koopman modes in representing the flow, by computing the error of the spectral-projection models. An n -dimensional spectral projection model, is an n -term truncation of the KMD where the modes are sorted based on their kinetic energy. The error defined as

$$\tilde{e}(n) = \frac{1}{T} \int_0^T \left\| \mathbf{u}(\mathbf{x}, t) - \sum_{k=1}^n \mathbf{u}_k(\mathbf{x}) e^{i\omega_k t} \right\| dt \quad (38)$$

gives the kinetic-energy norm of the difference between the spectral projection model (the sum in the above expression) and the actual flow field. Given the finite-dimensional nature of these models, they are essentially

quasi-periodic approximations of the flow. The time-averaged kinetic energy of the error for the spectral projections of order 1-10 is shown in FIG. 5. In the periodic and quasi-periodic flows, the bulk of the motion is readily captured by a few Koopman modes and the low-order projections approximate the flow with great accuracy. As the flow becomes less periodic with the increase of Reynolds number, the approximation error increases as well. For fully chaotic flows, the only Koopman mode is the mean flow and therefore there are no low-dimensional spectral projections except the steady one-dimensional model which is the mean flow itself. For purpose of comparison, however, we have plotted the error of spectral projections using Fourier modes (computed via FFT) at $Re=30000$. The kinetic energy of unsteady motion in this flow is spread in the continuous spectrum and any low-dimensional approximation using oscillatory components would involve large errors.

Figure 5 also shows an instructive comparison between Koopman mode decomposition and the Proper Orthogonal Decomposition (POD). POD is a decomposition of the flow field into spatially-orthogonal modes such that

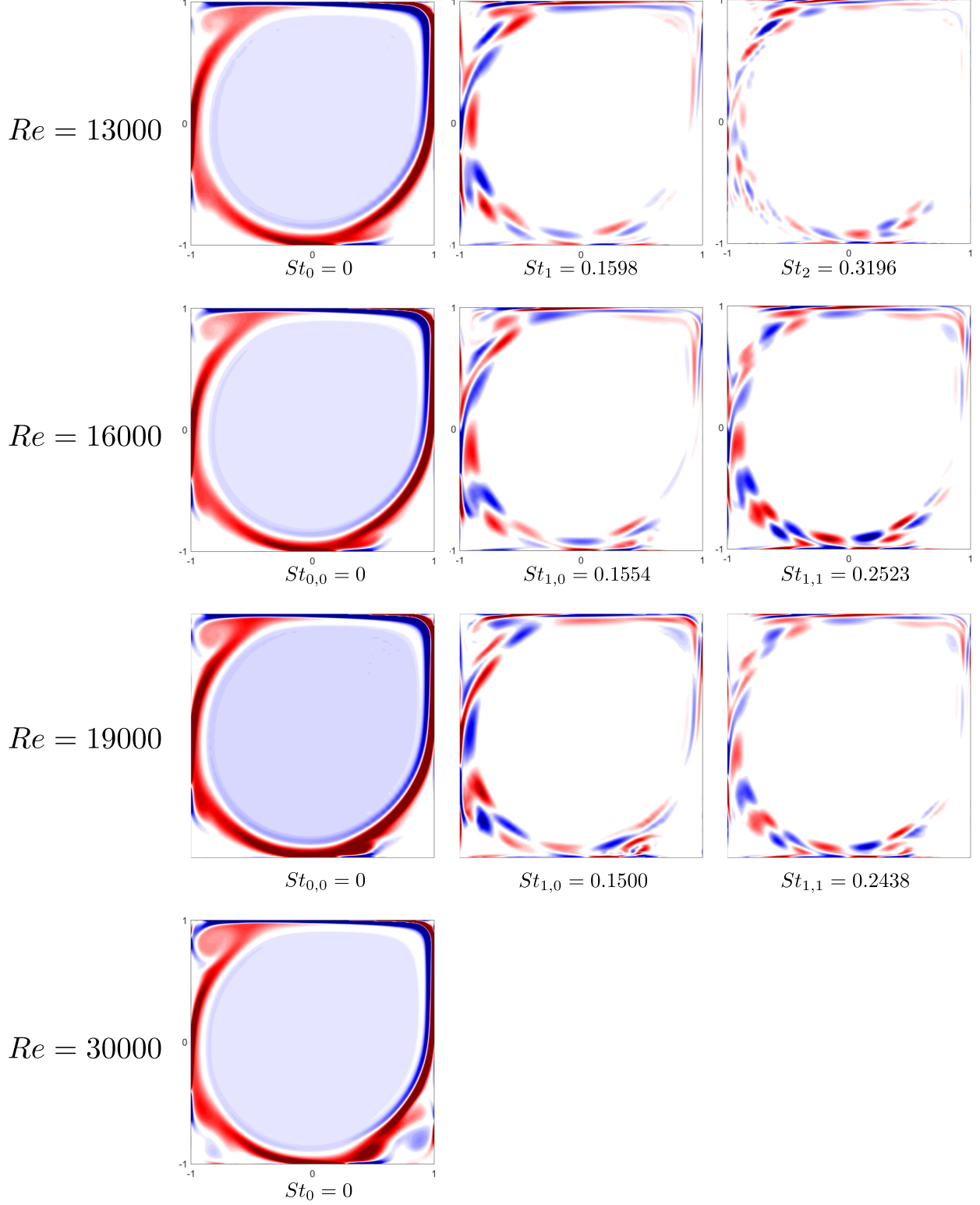


FIG. 4. The dominant Koopman modes of the cavity flow: The color field shows the real part of vorticity, with clockwise rotation shown in red, and counterclockwise in blue. The general structure of Koopman modes associated with same frequency trace remain unchanged as the Reynolds number is varied.

the POD-truncated models have the minimum energy error among all choices of orthogonal decompositions [58]. Due to its optimality and advantageous numerical properties, POD has been the keystone of many studies on coherent structures and low-order modeling of complex flows [59, 60]. POD has also been applied to the lid-driven cavity flow and previous studies have tested its performance in low-dimensional modeling of this flow [30, 33]. In case of periodic and quasi-periodic flow, the low-dimensional spectral projection model gives a better approximation of the flow than POD-truncated models (first two panels in FIG. 5). This observation is not contradictory to the optimality of POD-truncated models, but due to the fact that Koopman modes are potentially - and often for oscillating systems - complex-valued which allows for better representation of dynamics evolving on limit cycles or torus as previously suggested in Ref. 3 (see example 4 therein). For flows with mixed spectra, the error of approximation with spectral projection and POD is generally comparable but as the Reynolds number increases and the flow becomes more chaotic, POD-truncated models perform better. These observations support the alternative decomposition for model reduction proposed in Ref. 3, in which, the KMD is used to extract the periodic components of the flow, and then POD is used for representation of the remaining chaotic component.

V. CONCLUSION

We have proposed a new algorithm for computation of Koopman modes and frequencies in case of post-transient nonlinear flows. The algorithm is based on the rigorous theorems on convergence of harmonic averages and therefore capable of detecting genuine Koopman eigenvalues for flows with mixed spectra. Understanding of the asymptotic dynamics in the state space of the flow could be achieved by inspecting the distribution of the kinetic energy among the Koopman frequencies obtained by KMD of numerical data. In case of periodic or quasi-periodic attractors, the dominant Koopman frequencies occupy a lattice of values on the imaginary axis which is given by integral multiples of the basic frequencies corresponding to the motion of the state trajectory on the attractor. In contrast, chaotic flows show a significant growth of the kinetic energy contained within the continuous part of the Koopman spectrum. When both periodic and chaotic behavior are present in the numerical data, the method of harmonic averaging over varying windows could be used to delineate the peaks in the spectrum that correspond to periodic motion in the state space.

The Koopman mode decomposition shows great promise for low dimensional representation of complex flows. Study of unsteady lid-driven cavity flow shows

that in case of periodic and quasi-periodic flow, a handful of Koopman modes are sufficient to represent the spatio-temporal patterns with great accuracy. In fact, the Koopman modes offer a more efficient representation of periodic and quasi-periodic flows than POD modes. This is due to the fact that complex-valued Koopman modes are more suitable for describing the evolution on limit cycles and tori.

VI. ACKNOWLEDGEMENT AND SUPPLEMENTAL MATERIAL

This research was partially supported by the ONR grant N00014-14-1-0633. H.A. is grateful to Mohammad Nasr-Azadani for helpful comments on the manuscript, and Ati Sharma for a valuable discussion on POD.

The time series data and MATLAB codes for computation of KMD used to compute the results can be found at <https://ucsb.box.com/v/KMDofcavityflow>.

Appendix A: Some theorems from the Koopman Operator theory

In this section, we first recite the theorems that provide the general form of the Koopman mode decomposition for systems with stable periodic or quasi-periodic attractors. For a more detailed version of these theorems, including their proof, see Ref. 25.

Consider the dynamical system given by

$$\dot{\mathbf{x}} = \mathbf{F}(\mathbf{x}), \quad \mathbf{x} \in \mathcal{D} \subset \mathbb{R}^{n+1}, \quad \mathbf{F} \in C^2(\mathcal{D}) \quad (\text{A1})$$

which has a stable limit cycle with the basin of attraction \mathcal{B} . We can represent the dynamics in the basin of attraction \mathcal{B} using the linearized coordinate,

$$\begin{aligned} \dot{\mathbf{y}} &= A(s)\mathbf{y} \\ \dot{s} &= 1 \end{aligned} \quad (\text{A2})$$

$$\mathbf{y} \in \mathbb{R}^n, \quad s \in \mathbb{S}^1, \quad A(s + 2\pi) = A(s).$$

Since $A(s)$ is 2π -periodic, the solution (A2) is given by

$$\mathbf{y}(s) = \mathbf{P}(s)e^{s\mathbf{B}}\mathbf{y}(0), \quad (\text{A3})$$

where $\mathbf{P}(s)$ is 2π -periodic and $\mathbf{P}(0) = \mathbf{I}$. Let's denote the *Floquet exponents*, defined as eigenvalues of \mathbf{B} , by μ_i , $i = 1, 2, \dots, n$.

Theorem 1 (Koopman mode expansion for limit cycling systems) *Let the Floquet exponents μ_i , $i = 1, 2, \dots, n$ be distinct. Then any vector-valued observable $\mathbf{G}(\mathbf{y}, s) : \mathcal{B} \rightarrow \mathbb{R}^l$ which is analytic in \mathbf{y} and square integrable in s can be expanded in Koopman eigenfunctions of system (A2) as follows*

$$\mathbf{G}(\mathbf{y}, s) = \sum_{\mathbf{m} \in \mathbb{N}^n, k \in \mathbb{Z}} \mathbf{a}_{\mathbf{m}k} \mathbf{z}^{\mathbf{m}}(\mathbf{y}, s) e^{ik s} \quad (\text{A4})$$

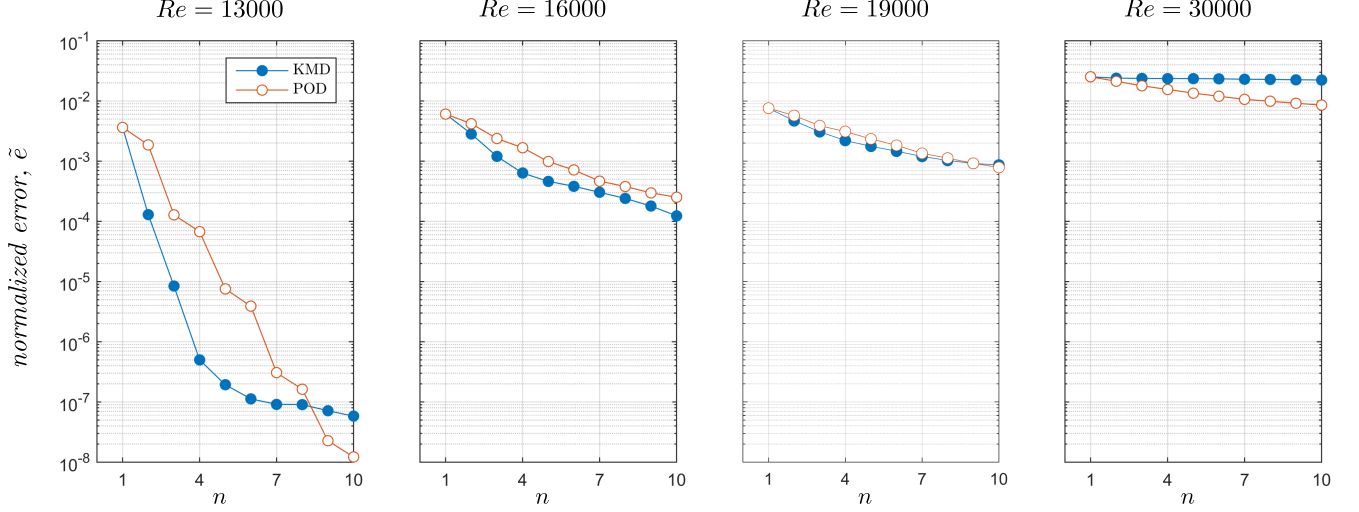


FIG. 5. The normalized kinetic energy of the error for approximation in Koopman mode decomposition (KMD) and Proper Orthogonal Decomposition (POD) as function of number of modes used in the approximation n . For $Re = 30000$ Fourier modes are used instead of Koopman oscillatory modes. Low-dimensional approximation with Koopman modes is more efficient in case of periodic and quasi-periodic flow.

where $\mathbf{a}_{\mathbf{m}k} \in \mathbb{R}^l$ are the Koopman modes, and

$$\mathbf{z}(\mathbf{y}, s) = (z_1(\mathbf{y}, s), \dots, z_k(\mathbf{y}, s))$$

are the principal Koopman eigenfunctions defined by

$$\mathbf{z}(\mathbf{y}, s) = \mathbf{V}^{-1} \mathbf{P}^{-1}(s) \mathbf{y}$$

where \mathbf{V}^{-1} diagonalizes the matrix \mathbf{B} . Moreover, $\mathbf{m} = (m_1, \dots, m_n)$ and a general Koopman eigenfunction is defined as

$$\mathbf{z}^{\mathbf{m}} = z_1^{m_1}(\mathbf{y}, s) \cdot \dots \cdot z_n^{m_n}(\mathbf{y}, s)$$

and associated with the Koopman eigenvalues $\mathbf{m} \cdot \boldsymbol{\mu} + ik$.

Now consider the more general case of a dynamical system with a stable quasi-periodic attractor. Assume that the dynamics on the attractor is conjugate to rotation m -dimensional torus \mathbb{T}^m given by

$$\dot{\boldsymbol{\theta}} = \boldsymbol{\omega}, \quad \boldsymbol{\omega} \in \mathbb{R}^m, \quad (\text{A5})$$

where frequencies in $\boldsymbol{\omega}$ are all incommensurable such that for every $\mathbf{k} \in \mathbb{Z}^m$, $\mathbf{k} \cdot \boldsymbol{\omega} \geq c/|\mathbf{k}|^\gamma$ for some $c, \gamma > 0$. Then the dynamics in basin of attraction for the attractor is conjugate to

$$\dot{\mathbf{y}} = A(\boldsymbol{\theta}) \mathbf{y} \quad (\text{A6})$$

$$\dot{\boldsymbol{\theta}} = \boldsymbol{\omega}$$

$$\mathbf{y} \in \mathbb{R}^n, \quad \boldsymbol{\theta} \in \mathbb{T}^m, \quad A(\boldsymbol{\theta} + 2\pi) = A(\boldsymbol{\theta}).$$

Define the matrices \mathbf{P} , \mathbf{B} similar to above and let quasi-Floquet exponents μ_i , $i = 1, 2, \dots, n$ be the eigenvalues of \mathbf{B} .

Theorem 2 (Koopman mode expansion for quasi-periodic systems) Assume the eigenvalues of the quasi-Floquet exponents are distinct. Then any vector-valued observable $\mathbf{G}(\mathbf{y}, \boldsymbol{\theta})$ which is analytic in \mathbf{y} and square integrable in $\boldsymbol{\theta}$ can be expanded in Koopman eigenfunctions of system (A6) as follows

$$\mathbf{G}(\mathbf{y}, \boldsymbol{\theta}) = \sum_{\mathbf{m} \in \mathbb{N}^n, \mathbf{k} \in \mathbb{Z}^m} \mathbf{a}_{\mathbf{m}k} \mathbf{z}^{\mathbf{m}}(\mathbf{y}, s) e^{i\mathbf{k} \cdot \boldsymbol{\theta}} \quad (\text{A7})$$

where $\mathbf{a}_{\mathbf{m}k}$ are Koopman modes, and $\mathbf{z}(\mathbf{y}, \boldsymbol{\theta}) = (z_1(\mathbf{y}, \boldsymbol{\theta}), \dots, z_k(\mathbf{y}, \boldsymbol{\theta}))$ denotes the principle Koopman eigenfunctions. Also

$$\mathbf{z}^{\mathbf{m}} = z_1^{m_1}(\mathbf{y}, s) \cdot \dots \cdot z_n^{m_n}(\mathbf{y}, s)$$

is a Koopman eigenfunction associated with the Koopman eigenvalue $\mathbf{m} \cdot \boldsymbol{\mu} + i\mathbf{k} \cdot \boldsymbol{\omega}$.

In case of post-transient flows with periodic or quasi-periodic attractor, we assume that the flow trajectory has converged onto the attractor and therefore the evolution of observables are given by expansions in (A4) and (A7) while setting $\mathbf{m} = 0$, which reduces the expansion to (8) and (10) used in this paper.

Next, we present two propositions regarding the Koopman mode decomposition of observables which are related through a linear operator or spatial differentiation.

Proposition 1 Let $g : M \rightarrow \mathbb{R}^n$ and $h : M \rightarrow \mathbb{R}^m$ be observables on a dynamical system which are related through the bounded linear operator \mathcal{D} such that $\mathcal{D}g = h$.

Let g_i and h_i denote the Koopman modes of observable g and h , respectively, at the Koopman eigenvalue λ_j . Then those modes are related to each other via $\mathcal{D}g_i = h_i$.

Proof: Let us assume for now that the dynamical system is measure-preserving which implies $\lambda_j = i\omega_j$, $\omega_j \in \mathbb{R}$. The Koopman modes are computed via the harmonic averaging and it follows that

$$\begin{aligned} h_j &= \lim_{T \rightarrow \infty} \frac{1}{T} \int_0^T h(t) e^{-i\omega_j t} dt \\ &= \lim_{T \rightarrow \infty} \frac{1}{T} \int_0^T \mathcal{D}g(t) e^{-i\omega_j t} dt \\ &= \lim_{T \rightarrow \infty} \frac{1}{T} \int_0^T g(t) e^{-i\omega_j t} dt \\ &= \mathcal{D} \lim_{T \rightarrow \infty} \frac{1}{T} \int_0^T g(t) e^{-i\omega_j t} dt \\ &= \mathcal{D} g_j \end{aligned} \quad (\text{A8})$$

We have used the linearity and continuity of \mathcal{D} in the 3rd and 4th equalities, respectively. If the system is dissipative, the Koopman modes are given by Generalized Laplace Analysis formula [24]. The above argument could be used, along with induction, to prove the statement for that case. \square

For the purposes of this paper, we are mostly interested in linear operators that involve spatial derivatives, such as gradient or curl. The derivative operator, however, is not bounded and therefore needs a special treatment which is given by the following proposition.

Proposition 2 *Let $g, h : \Omega \times M \rightarrow \mathbb{R}$ be two fields of observables defined on the flow domain Ω and the state space of the flow denoted by M . Assume the observables are bounded over their domain and related to each other through*

$$\mathcal{D}g = h, \quad (\text{A9})$$

where D denotes the partial derivative with respect to a spatial coordinate in the flow domain Ω . Let g_k and h_k denote the Koopman modes of observables associated with the Koopman frequencies ω_k , $k = 1, 2, \dots$. Then

$$\mathcal{D}g_k = h_k. \quad (\text{A10})$$

for every $x \in \Omega$.

Proof: Let's define the finite-time harmonic average of g at the frequency ω_k by

$$g_k^T(x) = \frac{1}{T} \int_0^T g(x, t) e^{-i\omega_k t} dt. \quad (\text{A11})$$

The Koopman mode of g associated with ω_k is then given by [3],

$$g_k = \lim_{T \rightarrow \infty} g_k^T. \quad (\text{A12})$$

$Re=13000$ (periodic)		$Re=16000$ (quasi-periodic)		$Re=19000$ (mixed spectra)	
St	k	St	k	St	k
0.00000	0	0.00000	(0, 0)	0.00000	(0, 0)
0.15983	1	0.15537	(1, 0)	0.24383	(1, 1)
0.31965	2	0.25229	(1, 1)	0.15005	(1, 0)
0.47947	3	0.09691	(0, 1)	0.20632	(2, -1)
0.63929	4	0.19381	(0, 2)	0.09378	(0, 1)
0.79913	5	0.31075	(2, 0)	0.18756	(0, 2)
0.95895	6	0.21383	(2, -1)	0.30010	(2, 0)
1.11879	7	0.34919	(1, 2)	0.05627	(1, -1)
1.27861	8	0.40767	(2, 1)	0.16881	(3, -3)
1.43843	9	0.05845	(1, -1)	0.33762	(6, -6)
1.59825	10	0.11695	(2, -2)	0.39389	(7, -7)
		0.13533	(-1, 3)	0.03751	(-1, 2)
		0.44609	(1, 3)	0.45016	(8, -8)
		0.29073	(0, 3)	0.48765	(2, 2)
		0.03843	(-1, 2)	0.28135	(5, -5)
		0.50457	(2, 2)	0.22508	(4, -4)
		0.23223	(-1, 4)	0.07502	(-2, 4)
		0.02005	(2, -3)	0.41264	(4, -2)
		0.46613	(3, 0)	0.35637	(3, -1)
		0.27235	(3, -2)	0.11254	(2, -2)

TABLE I. Koopman frequencies with highest kinetic energy in the lid-driven cavity flow

The Leibniz rule implies that the spatial derivative commutes with the finite-time averaging in (A11), i.e.,

$$h_k^T = \mathcal{D}g_k^T. \quad (\text{A13})$$

for any finite T . Now let's fix x . If both $h(x)$ and $g(x)$ are integrable functions, then the existence of $g_k(x)$ implies the existence of $h_k(x)$ [50], and since the scalar functions $h_k^T(x)$ and $\mathcal{D}g_k^T(x)$ are equal up to any finite T , their limits as $T \rightarrow \infty$ must be equal, i.e., $h_k(x) = \mathcal{D}g_k(x)$. \square

Appendix B: Discrete spectra of Koopman operator

Table I shows the Koopman frequencies of cavity flow obtained via algorithm in §III C. The basic frequency vector is $St = 0.15983$ for the flow at $Re=13000$, $St = [0.15537, 0.09691]$ for $Re=16000$ and $St = [0.15165, 0.09541]$ for $Re = 19000$. The rest of the frequencies can be described (typically to the sixth digit of accuracy) as a linear combination of the basic frequencies. The coefficients of the combination are given by k in the table.

Appendix C: Koopman eigenfunctions on embedded attractor

We have used the delay-embedding [61] of the kinetic energy observable (E) to plot the attractors of periodic and quasi-periodic flow in figure 2 and 3. Let the m -dimensional delay coordinates be defined as

$$E_{m,\tau}(t) = \begin{bmatrix} E(t) \\ E(t+\tau) \\ \vdots \\ E(t+(m-1)\tau) \end{bmatrix} \quad (C1)$$

where τ is the time delay. The embedded attractor in \mathbb{R}^m is visualized by plotting $E_{m,\tau}$ for the post-transient flow

at the sampling instants $[t_0, t_0 + \Delta t, \dots, t_0 + n\Delta t]$. We have chosen the parameter values $\tau = 1t_c$, $m = 2$, $\Delta t = 0.1t_c$ for the periodic flow, and $\tau = 2.4t_c$, $m = 3$, $\Delta t = 0.1t_c$ for the quasi-periodic flow.

Let $\phi_{\mathbf{k}}$ be the Koopman eigenfunction associated with the frequency $\omega_{\mathbf{k}}$. The (normalized) value of $\phi_{\mathbf{k}}$ at the above sampling times is given by

$$[e^{i\omega_{\mathbf{k}}t_0}, e^{i\omega_{\mathbf{k}}(t_0+\Delta t)}, \dots, e^{i\omega_{\mathbf{k}}(t_0+n\Delta t)}]. \quad (C2)$$

These values are plotted as color field on the embedded attractor using the `surface()` command in MATLAB.

-
- [1] B. O. Koopman, Proceedings of the National Academy of Sciences **17**, 315 (1931).
 - [2] I. Mezić and A. Banaszuk, Physica D: Nonlinear Phenomena **197**, 101 (2004).
 - [3] I. Mezić, Nonlinear Dynamics **41**, 309 (2005).
 - [4] Y. Susuki and I. Mezić, Power Systems, IEEE Transactions on **29**, 899 (2014).
 - [5] D. Giannakis, J. Slawinska, and Z. Zhao, in *Journal of Machine Learning Research, Proceedings of the 1st International Workshop on Feature Extraction: Modern Questions and Challenges and NIPS Conference*, Vol. 44 (2015) pp. 103–115.
 - [6] M. Georgescu and I. Mezić, Energy and buildings **86**, 794 (2015).
 - [7] N. B. Erichson, S. L. Brunton, and J. N. Kutz, arXiv preprint arXiv:1512.04205 (2015).
 - [8] B. W. Brunton, L. A. Johnson, J. G. Ojemann, and J. N. Kutz, Journal of neuroscience methods **258**, 1 (2016).
 - [9] J. Mann and J. N. Kutz, Quantitative Finance, **1** (2016).
 - [10] C. W. Rowley, I. Mezić, S. Bagheri, P. Schlatter, and D. S. Henningson, Journal of Fluid Mechanics **641**, 115 (2009).
 - [11] P. Schmid and J. Sesterhenn, in *In Sixty-First Annual Meeting of the APS Division of Fluid Dynamics* (2008).
 - [12] P. J. Schmid, Journal of Fluid Mechanics **656**, 5 (2010).
 - [13] P. J. Schmid, L. Li, M. Juniper, and O. Pust, Theoretical and Computational Fluid Dynamics **25**, 249 (2011).
 - [14] C. Pan, D. Yu, and J. Wang, Theoretical and Applied Mechanics Letters **1** (2011).
 - [15] A. Seena and H. J. Sung, International Journal of Heat and Fluid Flow **32**, 1098 (2011).
 - [16] T. W. Muld, G. Efraimsson, and D. S. Henningson, Computers & Fluids **57**, 87 (2012).
 - [17] J.-C. Hua, G. H. Gunaratne, D. G. Talley, J. R. Gord, and S. Roy, Journal of Fluid Mechanics **790**, 5 (2016).
 - [18] K. K. Chen, J. H. Tu, and C. W. Rowley, Journal of Nonlinear Science **22**, 887 (2012).
 - [19] S. Bagheri, J. Fluid Mech **726**, 596 (2013).
 - [20] T. Sayadi, P. J. Schmid, J. W. Nichols, and P. Moin, Journal of Fluid Mechanics **748**, 278 (2014).
 - [21] P. K. Subbareddy, M. D. Bartkowicz, and G. V. Candler, Journal of Fluid Mechanics **748**, 848 (2014).
 - [22] T. Sayadi, P. J. Schmid, F. Richecoeur, and D. Durox, Physics of Fluids **27**, 037102 (2015).
 - [23] B. Kramer, P. Grover, P. Boufounos, M. Benosman, and S. Nabi, arXiv preprint arXiv:1510.02831 (2015).
 - [24] I. Mezić, Annual Review of Fluid Mechanics **45**, 357 (2013).
 - [25] I. Mezić, arXiv preprint arXiv:1702.07597 (2017).
 - [26] H. L. Swinney and J. P. Gollub, Phys. Today **31** (1978).
 - [27] J. Laskar, C. Froeschlé, and A. Celletti, Physica D: Nonlinear Phenomena **56**, 253 (1992).
 - [28] J. Shen, Journal of Computational Physics **245**, 228 (1991).
 - [29] M. Poliashenko and C. K. Aidun, Journal of Computational Physics **121**, 246 (1995).
 - [30] W. Cazemier, R. Verstappen, and A. Veldman, Physics of Fluids (1994-present) **10**, 1685 (1998).
 - [31] F. Auteri, N. Parolini, and L. Quartapelle, Journal of Computational Physics **183**, 1 (2002).
 - [32] Y.-F. Peng, Y.-H. Shiau, and R. R. Hwang, Computers & Fluids **32**, 337 (2003).
 - [33] M. J. Balajewicz, E. H. Dowell, and B. R. Noack, Journal of Fluid Mechanics **729**, 285 (2013).
 - [34] M. O. Williams, I. G. Kevrekidis, and C. W. Rowley, Journal of Nonlinear Science **25**, 1307 (2015).
 - [35] J. N. Kutz, X. Fu, and S. L. Brunton, SIAM Journal on Applied Dynamical Systems **15**, 713 (2016).
 - [36] J. L. Proctor, S. L. Brunton, and J. N. Kutz, SIAM Journal on Applied Dynamical Systems **15**, 142 (2016).
 - [37] M. S. Hemati, M. O. Williams, and C. W. Rowley, Physics of Fluids **26**, 111701 (2014).
 - [38] F. Guéniat, L. Mathelin, and L. R. Pastur, Physics of Fluids **27**, 025113 (2015).
 - [39] S. L. Brunton, J. L. Proctor, and J. N. Kutz, arXiv preprint arXiv:1312.5186 (2013).
 - [40] J. H. Tu, C. W. Rowley, D. M. Luchtenburg, S. L. Brunton, and J. N. Kutz, Journal of Computational Dynamics (2014).
 - [41] S. T. Dawson, M. S. Hemati, M. O. Williams, and C. W.

- Rowley, *Experiments in Fluids* **57**, 1 (2016).
- [42] J. Laskar, *Icarus* **88**, 266 (1990).
 - [43] A. Wynn, D. Pearson, B. Ganapathisubramani, and P. Goulart, *Journal of Fluid Mechanics* **733**, 473 (2013).
 - [44] M. R. Jovanović, P. J. Schmid, and J. W. Nichols, *Physics of Fluids* (1994-present) **26**, 024103 (2014).
 - [45] G. Tissot, L. Cordier, N. Benard, and B. R. Noack, *Comptes Rendus Mécanique* **342**, 410 (2014).
 - [46] R. Temam, *Infinite-dimensional dynamical systems in mechanics and physics*, Vol. 68 (Springer-Verlag, 1988).
 - [47] P. R. Halmos, *Lectures on ergodic theory*, Vol. 142 (American Mathematical Soc., 1956).
 - [48] B. MacCluer, *Elementary functional analysis*, Vol. 253 (Springer Science & Business Media, 2008).
 - [49] L. N. Trefethen, *Spectral methods in MATLAB*, Vol. 10 (Siam, 2000).
 - [50] N. Wiener and A. Wintner, *American Journal of Mathematics* **63**, 415 (1941).
 - [51] I. Mezić and F. Sotiropoulos, *Physics of Fluids* (1994-present) **14**, 2235 (2002).
 - [52] U. Krengel and A. Brunel, *Ergodic theorems*, Vol. 59 (Cambridge Univ Press, 1985).
 - [53] S. Das and J. A. Yorke, arXiv preprint arXiv:1506.06810 (2015).
 - [54] G. A. Gottwald and I. Melbourne, *SIAM Journal on Applied Dynamical Systems* **8**, 129 (2009).
 - [55] Z. Levnajić and I. Mezić, *Chaos: An Interdisciplinary Journal of Nonlinear Science* **25**, 053105 (2015).
 - [56] H. Broer and F. Takens, *Archive for rational mechanics and analysis* **124**, 13 (1993).
 - [57] D. Ruelle and F. Takens, *Commun. math. phys* **20**, 167 (1971).
 - [58] G. Berkooz, P. Holmes, and J. L. Lumley, *Annual review of fluid mechanics* **25**, 539 (1993).
 - [59] B. R. Noack, K. Afanasiev, M. Morzynski, G. Tadmor, and F. Thiele, *Journal of Fluid Mechanics* **497**, 335 (2003).
 - [60] C. W. Rowley, T. Colonius, and R. M. Murray, *Physica D: Nonlinear Phenomena* **189**, 115 (2004).
 - [61] F. Takens, in *Dynamical systems and turbulence, Warwick 1980* (Springer, 1981) pp. 366–381.